

Article

# A Novel Method for Dynamic Molecular Weight Distribution Determination in Organometallic Catalyzed Olefin Polymerizations

Masoud Shiri <sup>1</sup>, Mahmoud Parvazinia <sup>1,\*</sup>, Ali Akbar Yousefi <sup>2</sup>, Naeimeh Bahri-Laleh <sup>1</sup>  and Albert Poater <sup>3,\*</sup> <sup>1</sup> Department of Engineering, Iran Polymer and Petrochemical Institute, Tehran 14965-115, Iran<sup>2</sup> Department of Polymer Processing, Iran Polymer and Petrochemical Institute, Tehran 14965-115, Iran<sup>3</sup> Institut de Química Computacional i Catàlisi, Departament de Química, Universitat de Girona, c/Maria Aurèlia Capmany 69, 17003 Girona, Spain

\* Correspondence: m.parvazinia@ippi.ac.ir (M.P.); albert.poater@udg.edu (A.P.)

**Abstract:** In this study, a mathematical model for the time evolution of molecular weight distribution (MWD) was developed. This temporal model is based on the well-known Ziegler–Natta polymerization mechanism and reaction kinetics by the parametric solving of related differential equations. However, due to the generality of the reactions involved, the model can be extended to the other type of catalysts, such as metallocenes, Phillips, etc. The superiority of this model lies in providing the possibility of a more precise prediction over the active sites and kinetic parameters using a simple mathematical equation, which leads to improved reactor design in large-scale production. The model uses a function to develop a methodology for MWD calculations. In this way, the transient response is limited to the first few minutes of the reaction; however, it is important as it demonstrates the establishment of the final MWD. According to the results, almost for practical conditions with negligible transfer resistances, the time dependency of the MWD has a transient interval, depending on the kinetic constants of polymerization reactions. Increasing the time to infinity results in an increase in MW and a widening in MWD, which confirms the experimental plots well. In short, the main advantage of our proposed model over the previous ones is its ability to predict the MWD even before the completion of the polymerization reaction. The results of the present model match well with those of the well-known Schulz–Flory distribution, which only predicts the final molecular weight distribution, thus confirming that the model is reliable and generalizable.

**Keywords:** molecular weight distribution; polyolefin; deconvolution; mathematical modeling; coordination polymerization



**Citation:** Shiri, M.; Parvazinia, M.; Yousefi, A.A.; Bahri-Laleh, N.; Poater, A. A Novel Method for Dynamic Molecular Weight Distribution Determination in Organometallic Catalyzed Olefin Polymerizations. *Catalysts* **2022**, *12*, 1130. <https://doi.org/10.3390/catal12101130>

Academic Editors: Diego Luna, Sergio Carrasco and Rebeca Martínez-Haya

Received: 31 August 2022

Accepted: 20 September 2022

Published: 28 September 2022

**Publisher's Note:** MDPI stays neutral with regard to jurisdictional claims in published maps and institutional affiliations.



**Copyright:** © 2022 by the authors. Licensee MDPI, Basel, Switzerland. This article is an open access article distributed under the terms and conditions of the Creative Commons Attribution (CC BY) license (<https://creativecommons.org/licenses/by/4.0/>).

## 1. Introduction

Polyolefins are one of the essential ingredients used in the production of artefacts such as pipes, tanks, polymer films, electrical conduits, electrical insulators, etc. [1–4]. Industrial catalytic production of polyolefins began in the early 1950s using Ziegler–Natta and Phillips catalysts. These catalysts were continuously improved to achieve higher yields, advanced particle morphology, and better control over the polymer microstructure [5–7]. In fact, despite the industrial success of metallocene catalysts in the late 1980s, Ziegler–Natta and Phillips catalysts remain the major contributors to the commercialization of polyolefins. Therefore, understanding how these catalysts produce polyolefins is important from both an industrial [8,9] and an academic point of view [10–14].

The kinetics of polymerization by Ziegler–Natta catalysts using simple mathematical models to predict the reaction rate and average molecular weight have been investigated previously [15–18]. However, an important property of the final polymer is molecular weight distribution (MWD), which affects many physical properties [19–21].

Several models were developed to predict the molecular weight distribution [22–24] and average molecular weight by using the method of moments as the most popular approach [25,26]. Kiparissides et al. [27] considered a generalized multisite mechanism to develop a mathematical model, simulating the polymer chain molecular characteristics during ethylene/alpha-olefin copolymerization in CSTRs (continuously stirred tank reactors).

MWD and short-chain branching distribution are usually modeled using two approaches: the method of moments and the Monte-Carlo algorithm [28]. Bontu developed a model for the micro- and meso-scale level of olefin polymerization using the method of moments. The model was based on the polymer flow model, alongside the intrinsic kinetic model obtained in the moments approach. In this model, the effect of mass transfer and kinetic parameters on the temperature profile and monomer concentration, and subsequently on the catalyst activity, polymer molecular weight [29–31] and MWD were examined [32]. Fan et al. developed a mathematical model for polymerization activity and active center concentrations in the first 5 min of polymerization. They found a two-stage kinetic for the formation of active centers. In addition, the polymer particle morphology and MWD were modeled as a function of time [33]. However, the suggested model was based on the catalyst active centers' behavior in the first 5 min of polymerization. Furthermore, Fan and coworkers studied the kinetics and mechanism of ethylene polymerization over a  $\text{TiCl}_4/\text{MgCl}_2$  catalyst. Here, the polymer MWD was determined in the first 10 min of polymerization considering the Ti content's effect on the number and structure of active sites formed [34].

There are some other models that were developed for MWD estimation at the end of polymerization [26,35,36]. The polymerization kinetics and the effect of reactor residence time on polymer microstructure, i.e., polymer molecular weight and MWD, were studied thoroughly by Soares et al. [37]. A dynamic model was developed to predict the polymer MWD, temperature profile, and polymer production rate in an industrial fluidized bed reactor during ethylene copolymerization [38]. In this model, the reactor parameters and polymer properties were estimated from the two-phase (bubble and emulsion) dynamic model. Chen et al. predicted the dynamic MWD during grade transition in a continuously stirred tank reactor. In this work, to improve the derived system of non-linear equations, a new moving finite element method was proposed [39]. Biegler and coworkers developed a model based on Flory distribution to predict the dynamic MWD of an industrial HDPE slurry process in CSTRs. This model was based on an equation-oriented (EO) framework. In this methodology, the parameter estimation problem was addressed [40]. Abedi et al. examined the influence of the polymerization time on the molecular weight and molecular weight distribution of Ziegler–Natta propylene polymerization [41]. Their results showed that the reaction time has a remarkable effect on the molecular weight and molecular weight distribution.

Existing experimental data show that, as the polymerization reaction proceeds, the MWD widens and the polymer molecular weight (MW) increases. This is not represented in the previous models as they only predict the final molecular weight. Therefore, in this research, we aimed to fill this gap. In this sense, a novel method was developed to determine the polymer molecular weight distribution (MWD) over time by using simple and comprehensive equations, as a key parameter in the modeling and prediction of the characteristics of the final polyolefin product.

## 2. Results and Discussion

The cumulative molecular weight distribution, based on Table 1 according to various references [25,42–47], is presented in Figure 1. We find that the cumulative molecular weight distribution curve is shifted to the left of the cumulative distribution curve at steady state (infinity time or Schulz–Flory distribution). This means that the average molecular weight increases with elapsing time until it reaches a steady-state situation and final distribution. Additionally, as seen in Figure 1, the molecular weight distribution is not totally developed

after 20 s from the beginning of the reaction. The most developed molecular length is about 1800, while, as time approaches infinity, this value approaches 10,000.

**Table 1.** Normal Range of Kinetic Constants.

Kinetic Constant	Acceptable Range
$k_p$	10–5000 s <sup>-1</sup> /(mol/L)
$k_i$	0–500 s <sup>-1</sup> /(mol/L)
$k_{t\beta}$	0–5 s <sup>-1</sup>
$k_{tH}$	0–1000 s <sup>-1</sup> /(mol/L)
$k_{tAl}$	0–50 s <sup>-1</sup> /(mol/L)
$k_{tM}$	0–100 s <sup>-1</sup> /(mol/L)
$k_d$	0–100 s <sup>-1</sup>
$k_{dI}$	0–1000 s <sup>-1</sup> /(mol/L)
[M]	0–30 mol/L
[H <sub>2</sub> ]	0–1 mol/L
[Al]	0–1 mol/L
[I]	0–1 mol/L
$K_p$	0–150,000 s <sup>-1</sup>
$K_I$	0–15,000 s <sup>-1</sup>
$K_T$	0–4000 s <sup>-1</sup>
$K_D$	0–1000 s <sup>-1</sup>

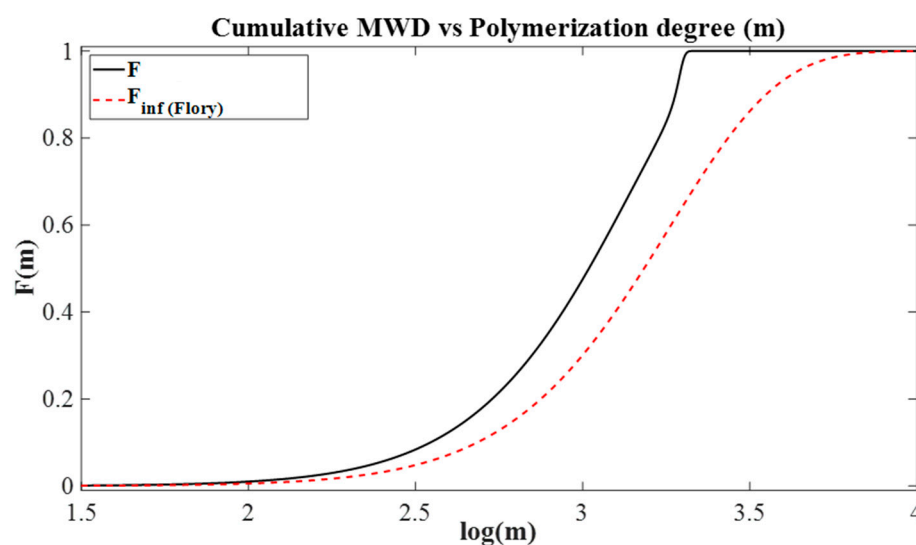


**Figure 1.** Cumulative molecular weight distribution according to Equations (33) and (34) ( $K_p = 100/s$ ,  $K_I = 1/s$ ,  $K_T = 0.1/s$ ,  $K_D = 0.01/s$ ,  $t = 20$  s).

The normalized differential distributions of Figure 1 are presented in Figure 2. As seen, by decreasing polymerization time, the peak height of molecular weight distribution increases, which means that the MWD becomes narrower (since the total area under the curve must be equal to 1). Additionally, similarly to Figure 1, since the molecular weight distribution cannot develop totally at the time 20 s, and the most developed molecular length is about 1800, one could see a spike in differential molecular weight distribution around a molecular length of 1800. By tending time to infinity, this spike completely disappears, because of the development of molecular weights.

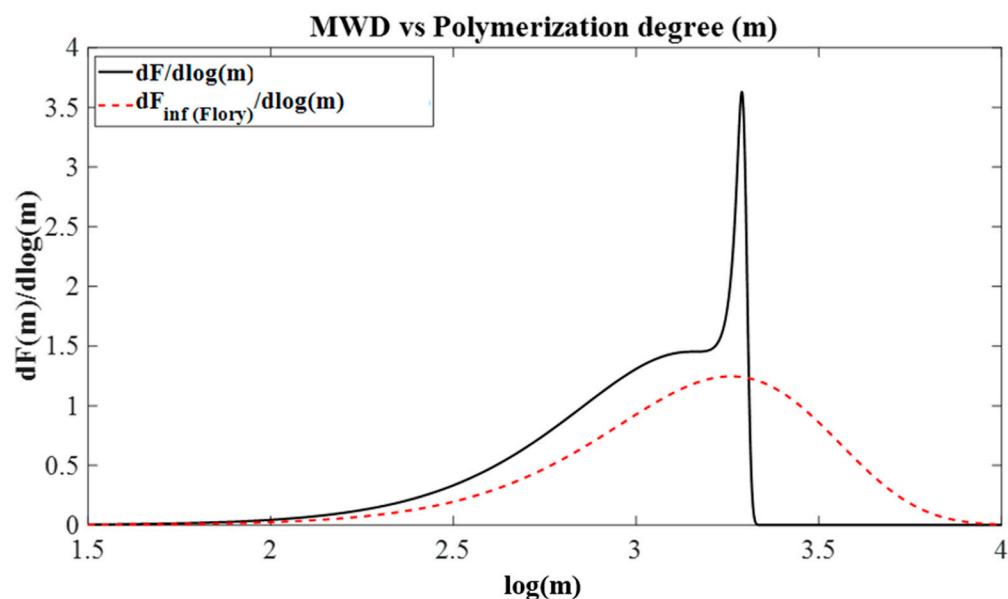


**Figure 2.** Molecular weight distribution according to Equations (33) and (34) ( $K_P = 100/s$ ,  $K_I = 1/s$ ,  $K_T = 0.1/s$ ,  $K_D = 0.01/s$ ,  $t = 20$  s).

As seen in Figures 1 and 2, according to selected kinetic constants, the time-dependent distribution is close to the steady-state distribution ( $F_{inf}$ ), even in the early stages. This reality is also obvious from the rapidly converging PDI to the final value (almost 2) in Figure 3. Therefore, if we ignore the first few minutes of reaction, when the molecular weight distribution function is identical and time-independent, only the number of polymer dead chains increases with time.

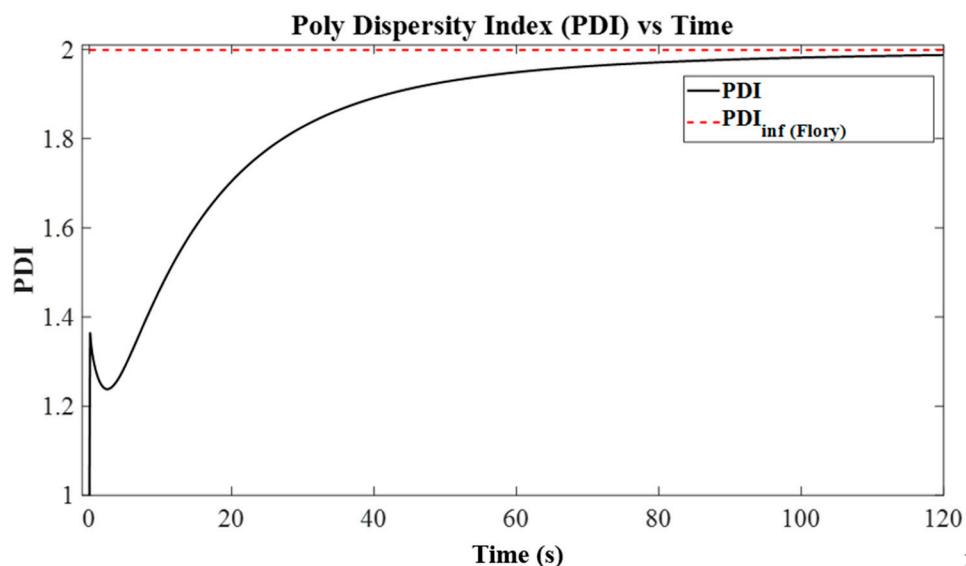


**Figure 3.** Polydispersity index according to Equations (36) and (37) ( $K_P = 100/s$ ,  $K_I = 1/s$ ,  $K_T = 0.1/s$ ,  $K_D = 0.01/s$ ).

Another parameter that cannot be described by Schulz–Flory distribution is the development of average molecular weight (or its twin, average molecular length). As seen in Figure 4, the average molecular length (or weight) increases with time to reach its steady value. This final value is predicted by Schulz–Flory distribution.

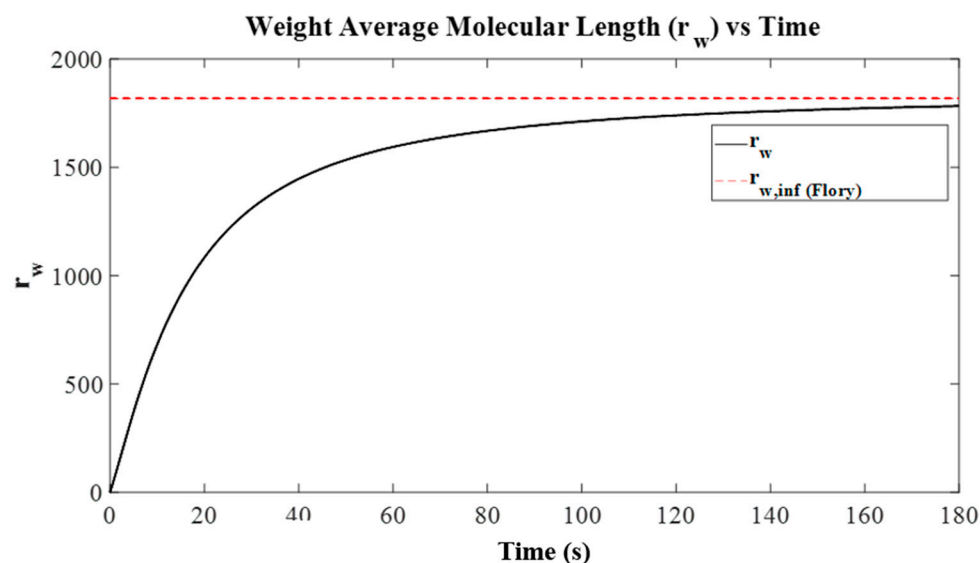


**Figure 4.** Weight average molecular length according to Equations (36) and (37) ( $K_P = 100/s$ ,  $K_I = 1/s$ ,  $K_T = 0.1/s$ ,  $K_D = 0.01/s$ ).

Cumulative MWD as a function of time is given in Figure 5. Obviously, as time goes on, the MWD approaches the Schulz–Flory distribution.

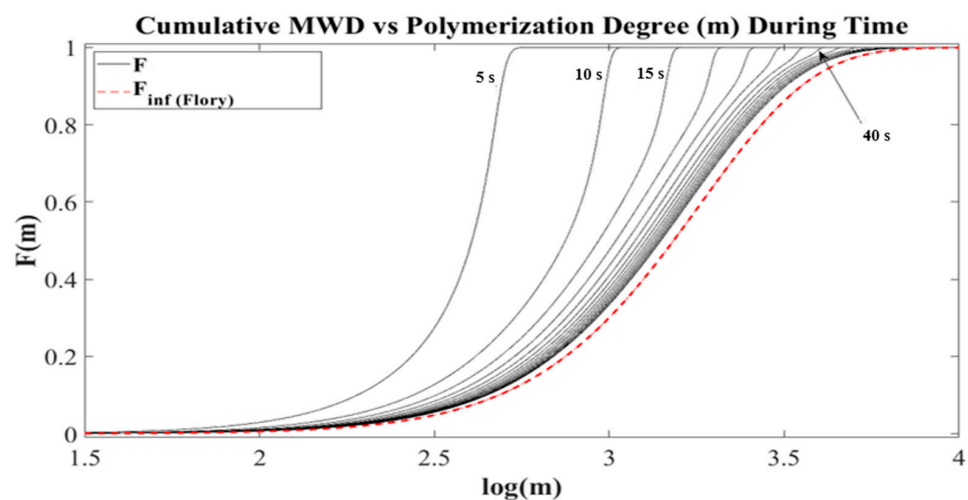


**Figure 5.** Cumulative molecular weight distribution according to Equations (36) and (37) ( $K_P = 100/s$ ,  $K_I = 1/s$ ,  $K_T = 0.1/s$ ,  $K_D = 0.01/s$ ,  $t = 5$  to  $75$  s by  $5$  s increments).

The molecular weight distribution is illustrated in Figure 6. The peak of distribution approaches the higher molecular weights values and finally reaches the Schulz–Flory distribution. In fact, the main advantage of this model is its ability to predict the molecular weight distribution during the polymerization reaction. Although the transition period is less than a few minutes, according to the values of  $K_P$ ,  $K_I$ ,  $K_T$ , and  $K_D$ , it may rarely exist for an hour or more; however, in commercial catalysts, this period is very short.

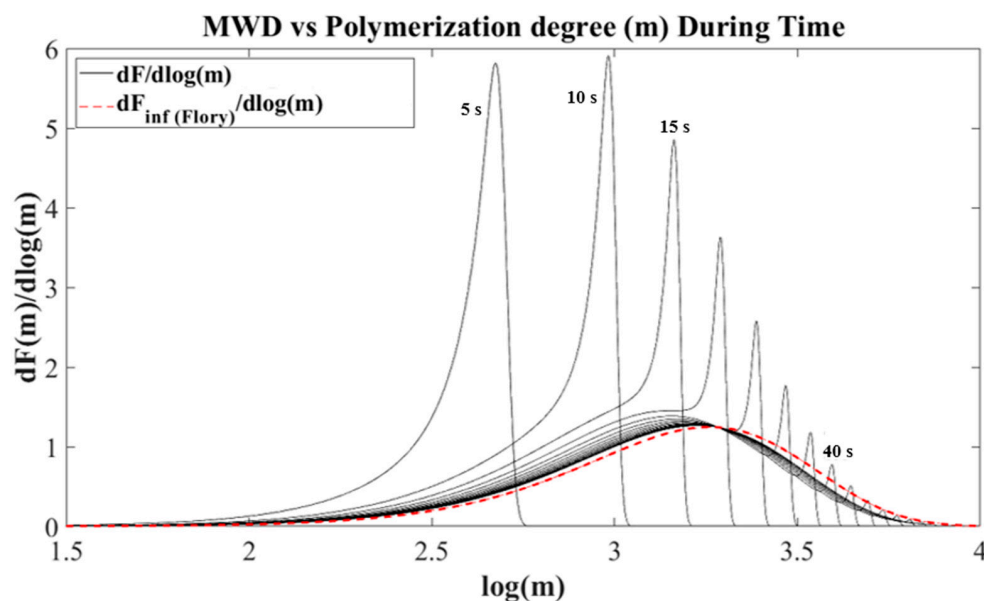


**Figure 6.** Molecular weight distribution according to Equations (33) and (34) ( $K_P = 100/s$ ,  $K_I = 1/s$ ,  $K_T = 0.1/s$ ,  $K_D = 0.01/s$ ,  $t = 5$  to  $75$  s by  $5$  s increments).

Gel permeation chromatography (GPC) instruments often express a weight distribution of molecular weight, using Equation (34) discussed in the Materials and Methods Section, which we may write as:

$$\frac{dF_{\infty}(m)}{d \log(m)} = \frac{dF_{\infty}(m)}{d \log(m/dm)} = -(m \ln 10) \left[ m + (m^2 + Q)(1 - Q) \right] Q^{m-1} \quad (1)$$

Additionally, from Equation (37) we have:

$$\bar{r}_n = \frac{1}{1 - Q} \rightarrow Q = 1 - \frac{1}{\bar{r}_n} \quad (2)$$

Using Equations (1) and (2), one could deconvolute a real final GPC curve of a sample [25,48–51]. As an example, the GPC graph of a polypropylene produced by conventional  $MgCl_2$ -supported  $TiCl_4$  catalyst [51], deconvoluted using our proposed method, is shown in Figure 7. For the aforementioned GPC curve, the deconvolution results are given in Table 2.

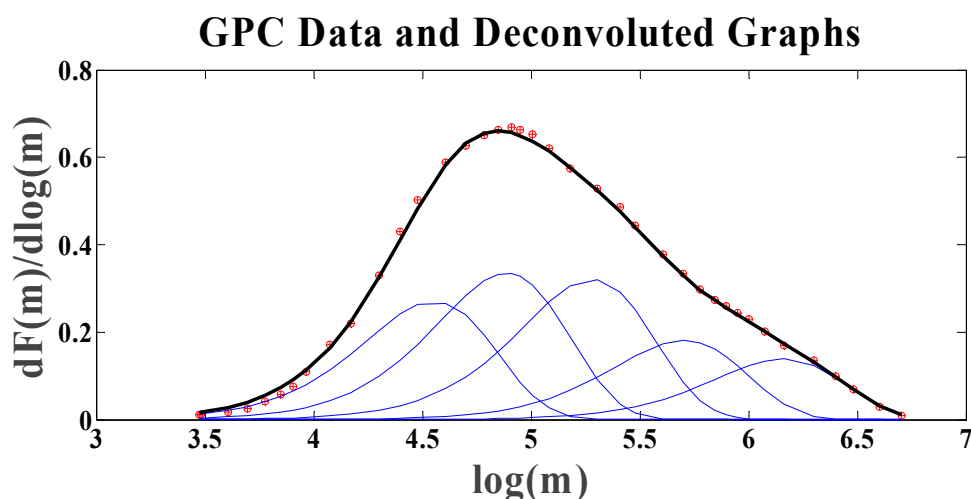


**Figure 7.** Deconvoluted GPC curve of a typically produced polypropylene.

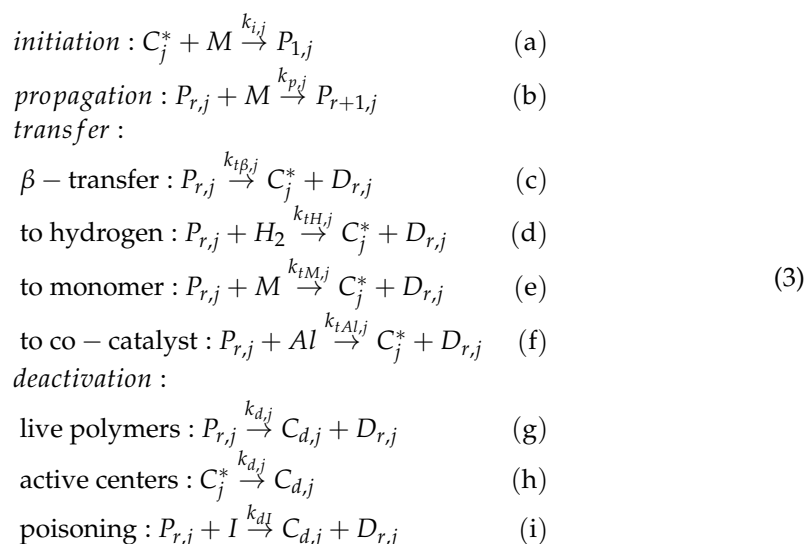
**Table 2.** Molecular Weight Distribution Deconvolution Result.

	Site 1	Site 2	Site 3	Site 4	Site 5
Weight Percentage of Each Site	21.88	27.18	26.02	14.70	10.22
$M_{n,avg}$ (g/mol)	17,940	38,690	95,430	252,470	724,230
$M_{w,avg}$ (g/mol)	35,877	77,377	190,860	504,940	1,448,500

Note that the weight percentage of each site presented in Table 2 is the weight percentage of the polymer produced by that catalyst site. Determining the weight percentage of individual sites requires the kinetic constants ( $K_P$ ,  $K_I$ ,  $K_T$ , and  $K_D$ ) for each site type, and is beyond the scope of this paper.

### 3. Materials and Methods

The MWD model developed here is based on the method of moments equations. There are several proposed kinetic mechanisms and equations in the literature [52–54], but the most accepted one for single- or multi-site polymerization of  $\alpha$ -olefins by Ziegler–Natta catalysts is as follows [55]:



where  $M$  represents the concentration of  $\alpha$ -olefin monomer;  $C_j^*$  and  $C_{d,j}$  represent the vacant active site and deactivated site of type  $j$ ; and  $P_{r,j}$  and  $D_{r,j}$  represent living and dead polymer with chain length of  $r$  associated with the active site of type  $j$ , respectively. In addition,  $Al$  denotes the concentration of aluminum alkyl and  $H_2$  represents the concentration of hydrogen, which is the most important transfer agent in Ziegler–Natta polymerization that significantly controls the molecular weight and, in some situations, the rate of polymerization [42,56]. Moreover, the chain transfer to hydrogen and aluminum alkyl (co-catalyst) is shown through the transfer reactions proportional to the square root of the concentration of transfer agents [50,55,57]. The complicated poisoning process is simplified in this model, such that it cannot considerably deteriorate the accuracy of the model [43]. In addition, the activation process is very fast; thus, it is assumed that before the catalyst enters the reactor, it is activated and therefore the role of  $Al$  in transfer reactions appears.

Note that this scheme represents kinetics of each type of the active sites individually without any interrelation. Although this mechanism is well accepted in polymerization reaction modeling, its microstructural simulation ability is limited [55]. It is worth mentioning that the main difference between single-site and multi-site models is the presence of linear summation over the number of active sites in the latter. The number of active centers is usually from two to five and one could easily expand the single-site catalyst equations to a multi-site catalyst by methods of linear algebra and the superposition of physical phenomena.

Moreover, the aforementioned mechanism shows that the chain growth is initiated by the insertion of the first monomer to the active site, followed by chain propagation. In addition, the chain transfer reactions, which include spontaneous beta chain transfer, transfer to hydrogen, transfer to monomer, and transfer to co-catalyst, occur simultaneously, leading to the production of dead polymer chains. In addition, these chains can be produced through growing chain deactivation or reaction with poisons and impurities. Additionally, each active site may undergo a deactivation reaction [51,55,58,59], which goes against the goal of a high catalyst reuse [60–63].

A few assumptions have been made in the polymerization mechanism to simplify the next derivations, which are as the following:

1. Site activation by alkyl aluminum assumed to be instantaneous (i.e., reaction between catalyst and co-catalyst). Therefore, the site activation mechanism was ignored.
2. Transfer reactions assumed to form the same site type,  $C^*$ , which originally formed by activation of catalyst with the co-catalyst.

Using Equation (1) and its sub-equations, the material balance equations can be written as follows. Note that to avoid unnecessary complexity, one site equation is written without index  $j$ , and, as stated before, they could be integrated easily for a multi-site model. Therefore, we have:

$$\begin{aligned} \frac{dP_r}{dt} &= k_p M (P_{r-1} - P_r) - (k_{t\beta} + k_{tH} H_2 + k_{tAl} Al + k_{tM} M + k_{dI} I + k_d) P_r \\ \text{or simply } \frac{dP_r}{dt} &= K_P P_{r-1} - (K_P + K_T + K_D) P_r \end{aligned} \quad (4)$$

Moreover, for the chain length of one, it is a bit different:

$$\frac{dP_1}{dt} = K_I C^* - (K_P + K_T + K_D) P_1 \quad (5)$$

For dead polymer chains we could write:

$$\frac{dD_r}{dt} = (k_{t\beta} + k_{tH} H_2 + k_{tAl} Al + k_{tM} M + k_{dI} I + k_d) P_r = (K_T + K_D) P_r \quad (6)$$

where  $K_P$ ,  $K_T$ ,  $K_I$ , and  $K_D$  are

$$\begin{aligned} K_P &= k_p M & (a) \\ K_I &= k_i M & (b) \\ K_T &= (k_{t\beta} + k_{tH} H_2 + k_{tAl} Al + k_{tM} M) & (c) \\ K_D &= (k_{dI} I + k_d) & (d) \end{aligned} \quad (7)$$

Additionally, for  $C^*$  we have:

$$\frac{dC^*}{dt} = -(K_I + K_D) C^* + K_T Y_0 \quad (8)$$

To make further calculations easier, we define a variable, named  $P_0$ , by the following formula:

$$P_0 = (K_I / K_P) C^* \text{ equivalent to } K_P P_0 = K_I C^* \quad (9)$$

The substitution of Equation (9) in Equation (5) leads to:

$$\frac{dP_1}{dt} = K_P P_0 - (K_P + K_T + K_D) P_1 \quad (10)$$

This is similar to Equation (4) for higher-order living polymer chains equations. Additionally, assuming constant values for  $K_P$  and  $K_I$ , Equation (8) can be rewritten as:

$$\frac{dP_0}{dt} = -(K_I + K_D) P_0 + \frac{K_I}{K_P} K_T Y_0 \quad (11)$$

In addition,  $Y_0$  is the zero moment of living polymer chain distribution and using the general definition of  $q$ th moment of a distribution function  $f(x)$  by:

$$\mu_q = \sum_{x=1}^{\infty} x^q f(x)$$

This leads to:

$$Y_0 = \sum_{r=1}^{\infty} P_r$$

Considering this definition, we obtain

$$\frac{dY_0}{dt} = \frac{dP_1}{dt} + \sum_{r=2}^{\infty} \frac{dP_r}{dt}$$

Additionally, using Equations (4) and (5), we easily show that:

$$\frac{dY_0}{dt} = K_I C^* - (K_T + K_D)Y_0 = K_P P_0 - (K_T + K_D)Y_0 \quad (12)$$

In addition [23],

$$\frac{dY_1}{dt} = K_I C^* + K_P Y_0 - (K_T + K_D)Y_1 = K_P P_0 + K_P Y_0 - (K_T + K_D)Y_1 \quad (13)$$

$$\frac{dY_2}{dt} = K_I C^* + K_P Y_0 + 2K_P Y_1 - (K_T + K_D)Y_2 = K_P P_0 + K_P Y_0 + 2K_P Y_1 - (K_T + K_D)Y_2 \quad (14)$$

Similar equations could be written for dead polymer chains distribution by denoting  $X_q$  as  $q$ th moment of dead polymer chains distribution. Therefore, we have:

$$\frac{dX_q}{dt} = \sum_{r=1}^{\infty} r^q \frac{dD_r}{dt} = \sum_{r=1}^{\infty} (K_T + K_D)r^q P_r = (K_T + K_D)Y_q \quad (15)$$

Or, for zero to second moments, we could write:

$$\begin{aligned} \frac{dX_0}{dt} &= (K_T + K_D)Y_0 & (a) \\ \frac{dX_1}{dt} &= (K_T + K_D)Y_1 & (b) \\ \frac{dX_2}{dt} &= (K_T + K_D)Y_2 & (c) \end{aligned} \quad (16)$$

Equations (8)–(16) can be written as a linear first-order ordinary differential equation by using a matrix form of differential equations. However, it should be noted that the values of  $K_P$ ,  $K_I$ ,  $K_D$ , and  $K_T$  are functions of time. The concentrations of monomer, hydrogen, other transfer agents, and impurities are not constant in the different positions of a growing polymer particle. In addition, the rate parameters are not constant over the growing particle because the temperature differs in practice in different positions of a growing polymer particle under the reaction conditions. However, in some cases of mild conditions of slurry ethylene or propylene polymerization, the temperature gradient inside the growing particle could be neglected and concentrations could remain approximately constant.

Note that the average molecular weights of polymerization and dispersity ( $PDI$ ) could be found by the following Equations [64]:

$$\bar{M}_w = mw \frac{X_2 + Y_2}{X_1 + Y_1} = mw \frac{Z_2}{Z_1} \quad (17)$$

$$\bar{M}_n = mw \frac{X_1 + Y_1}{X_0 + Y_0} = mw \frac{Z_1}{Z_0} \quad (18)$$

$$PDI = \frac{\bar{M}_w}{\bar{M}_n} = \frac{(X_2 + Y_2)(X_0 + Y_0)}{(X_1 + Y_1)^2} = \frac{Z_2 Z_0}{Z_1^2} \quad (19)$$

In Equations (17) and (18),  $m_w$  denotes the molecular weight of monomer. In most polymerization reactions, dead polymer moments are much bigger than their corresponding live moment ( $X_j \gg Y_j$ ) [43,54], so sometimes in Equations (17)–(19), live moments can be ignored.

Since the main purpose of this research is to develop a methodology for the molecular weight distribution calculation, the following equation is presented:

$$f(m) = \frac{\text{weight of polymer with chain lengths from } m + 1 \text{ to } \infty}{\text{total weight of polymer}} = 1 - F(m) \tag{20}$$

In Equation (20),  $F(m)$  denotes the cumulative distribution of molecular weight. By such definition of  $f(m)$  we could easily write:

$$f(m) = \frac{\sum_{r=m+1}^{\infty} r(P_r + D_r)}{\sum_{r=1}^{\infty} r(P_r + D_r)} = \frac{\sum_{r=m+1}^{\infty} r(P_r + D_r)}{Y_1 + X_1} \tag{21}$$

Therefore, by differentiating Equation (21) we have:

$$\frac{df(m)}{dt} = \dot{f}(m) = \frac{\sum_{r=m+1}^{\infty} r(\dot{P}_r + \dot{D}_r)}{Y_1 + X_1} - \frac{\dot{Y}_1 + \dot{X}_1}{Y_1 + X_1} f(m) \tag{22}$$

It is obvious from Equation (22) that by finding an expression for  $\sum_{r=m+1}^{\infty} r(\dot{P}_r + \dot{D}_r)$ , an equation for the molecular weight distribution is obtained. By simultaneous solution of this equation with the moment differential equations, time distribution of molecular weight is achieved. Using Equations (4), (6), and (10):

$$\begin{aligned} \sum_{r=m+1}^{\infty} r(\dot{P}_r + \dot{D}_r) &= \sum_{r=m+1}^{\infty} r\{[K_P P_{r-1} - (K_P + K_T + K_D)P_r] + [(K_T + K_D)P_r]\} \\ \Rightarrow \sum_{r=m+1}^{\infty} r(\dot{P}_r + \dot{D}_r) &= K_P \sum_{r=m+1}^{\infty} r(P_{r-1} - P_r), \quad m \geq 1 \end{aligned} \tag{23}$$

By manipulating Equation (23), along with some simplification, the results show that:

$$\sum_{r=m+1}^{\infty} r(\dot{P}_r + \dot{D}_r) = K_P[(m + 1)P_m + (P_{m+1} + P_{m+2} + \dots + P_{\infty})] = K_P \left[ mP_m + \sum_{r=m}^{\infty} P_r \right] \tag{24}$$

Writing the above equation in matrix form together with some algebraic manipulations, Equations (25) and (26) are finally obtained:

$$C^* = \frac{C_0^*}{K_I + K_T} \left[ K_T e^{-K_D t} + K_I e^{-(K_I + K_T + K_D)t} \right] \tag{25}$$

Additionally,

$$Y_0 = \frac{C_0^*}{K_I + K_T} K_I \left[ e^{-K_D t} - e^{-(K_I + K_T + K_D)t} \right] \tag{26}$$

Deriving molecular weight distribution equation needs defining  $X_1, Y_1, \dot{X}_1, \dot{Y}_1$ , and the right-hand term in Equation (24) is defined as:

$$A(t) = K_P \left[ mP_m + \sum_{r=m}^{\infty} P_r \right]$$

This is performed by the Laplace transform, which finally yields:

$$\begin{aligned} A(s) &= \frac{K_I C_0^*}{K_I + K_T} G(s) H(s) \text{ in which} \\ G(s) &= \left[ (m + 1) + \frac{K_P}{(K_T + K_D) + s} \right] \left[ \frac{K_T}{K_D + s} + \frac{K_I}{(K_I + K_T + K_D) + s} \right] \\ H(s) &= \left[ \frac{K_P}{(K_P + K_T + K_D) + s} \right]^m \end{aligned} \tag{27}$$

The equation can be written in time domain as:

$$\begin{aligned}
 A(t) &= \mathcal{L}^{-1}A(s) = \frac{K_I C_0^*}{K_I + K_T} \int_0^t G(t - \tau)H(\tau)d\tau \\
 &= \frac{K_I C_0^*}{K_I + K_T} \frac{K_P^m}{(m-1)!} \left\{ \begin{aligned} &[(m + 1)K_T + K_P]e^{-K_D t} \int_0^t \tau^{m-1} e^{-(K_P + K_T)\tau} d\tau \\ &+ [(m + 1)K_I - K_P]e^{-(K_I + K_T + K_D)t} \int_0^t \tau^{m-1} e^{-(K_P - K_I)\tau} d\tau \end{aligned} \right\} \quad (28)
 \end{aligned}$$

Referring to the definition of the lower, incomplete Gamma function ( $\gamma$  function), we may write:

$$A(t) = \frac{K_I C_0^*}{(K_I + K_T)(m-1)!} \left\{ \begin{aligned} &[(m + 1)K_T + K_P] \left(\frac{K_P}{K_P + K_T}\right)^m e^{-K_D t} \gamma(m, (K_P + K_T)t) \\ &+ [(m + 1)K_I - K_P] \left(\frac{K_P}{K_P - K_I}\right)^m e^{-(K_I + K_T + K_D)t} \gamma(m, (K_P - K_I)t) \end{aligned} \right\} \quad (29)$$

Now, to find  $f(m,t)$ , we refer to Equation (22), which could be written as:

$$\frac{df(m,t)}{dt} = \dot{f}(m,t) = \frac{A(t)}{Y_1 + X_1} - \frac{\dot{Y}_1 + \dot{X}_1}{Y_1 + X_1} f(m,t) = \frac{A(t)}{Z_1(t)} - \frac{\dot{Z}_1(t)}{Z_1(t)} f(m,t) \quad (30)$$

Since Equation (30) is a linear first-order ordinary differential equation, it could be easily solved by finding its integral factor, as follows:

$$f(m,t) = \frac{\int_0^t A(\tau)d\tau + C(m)}{Z_1(t)} \quad (31)$$

At the beginning of the polymerization (time zero), there is no live or dead polymer chain; therefore, the value of  $F(m,t) = 1 - f(m,t)$  must be equal to 1 for every  $m$  equal to or bigger than 1. Therefore,  $C(m)$  must be zero for every  $m \geq 1$ .

Now the remaining parameter to find the molecular weight distribution is the sum of the live and dead first polymer moments (value of  $Z_1$ ), which finally results in:

$$Z_1(t) = Y_1(t) + X_1(t) = \left(\frac{K_I C_0^*}{K_I + K_T}\right) \left\{ \frac{K_I - K_P}{K_I + K_T + K_D} [1 - e^{-(K_I + K_T + K_D)t}] + \frac{K_P + K_T}{K_D} (1 - e^{-K_D t}) \right\} \quad (32)$$

In that way, combining Equations (20), (29), (31), and (32), we may write:

$$F(m,t) = 1 - \frac{\left\{ \begin{aligned} &\frac{[(m+1)K_T + K_P]}{K_D(m-1)!} \left[ \begin{aligned} &\left(\frac{K_P}{K_P + K_T + K_D}\right)^m \gamma(m, (K_P + K_T + K_D)t) \\ &- \left(\frac{K_P}{K_P + K_T}\right)^m e^{-K_D t} \gamma(m, (K_P + K_T)t) \end{aligned} \right] \\ &+ \frac{[(m+1)K_I - K_P]}{(K_I + K_T + K_D)(m-1)!} \left[ \begin{aligned} &\left(\frac{K_P}{K_P + K_T + K_D}\right)^m \gamma(m, (K_P + K_T + K_D)t) \\ &- \left(\frac{K_P}{K_P - K_I}\right)^m e^{-(K_I + K_T + K_D)t} \gamma(m, (K_P - K_I)t) \end{aligned} \right] \end{aligned} \right\}}{\left\{ \frac{K_P + K_T}{K_D} (1 - e^{-K_D t}) + \frac{K_I - K_P}{K_I + K_T + K_D} [1 - e^{-(K_I + K_T + K_D)t}] \right\}} \quad (33)$$

At the end of the reaction:

$$\begin{aligned}
 F(m,t = \infty) &= 1 - \frac{\left\{ \frac{[(m+1)K_T + K_P]}{K_D} \left(\frac{K_P}{K_P + K_T + K_D}\right)^m + \frac{[(m+1)K_I - K_P]}{(K_I + K_T + K_D)} \left(\frac{K_P}{K_P + K_T + K_D}\right)^m \right\}}{\left\{ \frac{K_P + K_T}{K_D} + \frac{K_I - K_P}{K_I + K_T + K_D} \right\}} \\
 \Rightarrow F(m,t = \infty) &= 1 - \left[ 1 + m \left( 1 - \frac{K_P}{K_P + K_T + K_D} \right) \right] \left( \frac{K_P}{K_P + K_T + K_D} \right)^m \\
 \Rightarrow F(m,t = \infty) &= 1 - [1 + m(1 - Q)]Q^m
 \end{aligned} \quad (34)$$

It is obvious from Equation (34) that the final molecular weight distribution is identical to the one predicted by Schulz–Flory distribution [64].  $Q$  is the growth probability.

$$PDI = \frac{\overline{M}_w}{\overline{M}_n} = 1 + Q = 1 + \frac{K_P}{K_P + K_T + K_D} \quad (35)$$

Equation (35) shows that polydispersity index is between one and two for single site polymerization; this is a bit less than the value two, which was reported before, based on Flory's most probable distribution of chain lengths [48,58,59]. Therefore, Equation (35) once again confirms the validity of the proposed methodology.

The average molecular weight and  $PDI$  can be derived with respect to the presented model as:

$$\begin{aligned} \overline{M}_w &= mw \frac{(x-1)(2x-1)A - 2(x+y)B + (y+1)(2y+1)C}{(1-x)A + (1+y)C} \\ \overline{M}_n &= mw \frac{(1-x)A + (1+y)C}{A+C} \\ PDI &= \frac{[(x-1)(2x-1)A - 2(x+y)B + (y+1)(2y+1)C](A+C)}{[(1-x)A + (1+y)C]^2} \\ A &= K_I \frac{1 - e^{-(K_I + K_T + K_D)t}}{K_I + K_T + K_D}, \quad B = K_P \frac{1 - e^{-(K_T + K_D)t}}{K_T + K_D}, \quad C = K_T \frac{1 - e^{-K_D t}}{K_D} \\ x &= \frac{K_P}{K_I}, \quad y = \frac{K_P}{K_T}, \quad \lim_{t \rightarrow 0} PDI = 1 \end{aligned} \quad (36)$$

Although from Equation (34) we expect that, when time tends to infinity, the values of average molecular weights and polydispersity are identical to equations derived by Schulz–Flory distribution; however, by simplifying Equation (36), we could write:

$$\overline{M}_w|_{t=\infty} = mw \frac{1+Q}{1-Q}, \quad \overline{M}_n|_{t=\infty} = mw \frac{1}{1-Q}, \quad PDI|_{t=\infty} = 1 + Q \quad (37)$$

where  $Q = \frac{K_P}{K_P + K_T + K_D}$

This is identical to the previous equations and justifies the validity of the proposed methodology and derived equations.

#### 4. Conclusions

A new protocol for time-dependent molecular weight distribution estimation was developed for catalytic olefin polymerizations, using traditional heterogeneous Ziegler–Natta, metallocene, and Phillips catalysts. The proposed method, in addition to its practical characteristics, can estimate molecular weight and its distribution at any time of olefin polymerization experiments. According to the method, the molecular weight distribution at infinity obeys the well-known Schulz–Flory distribution, but the polymerization progresses especially at the initial times, resulting in a deviation from Schulz–Flory distribution. Our model predicts both the molecular weight increase and molecular weight distribution widening, which confirms the experimentally observed trend well. This affirms the reliability and generalizability of the proposed model. Our next goal is to extend the methodological results to other metal-catalyzed olefin polymerizations, as well as other, more complex substrates.

**Author Contributions:** Conceptualization, M.P., N.B.-L. and A.P.; data curation, M.S., M.P. and A.A.Y.; formal analysis, M.S., A.A.Y. and N.B.-L.; funding acquisition, A.P.; investigation, M.S., M.P. and A.A.Y.; methodology, M.S., M.P. and A.A.Y.; validation, M.S. and N.B.-L.; visualization, A.A.Y.; writing—original draft preparation, M.S.; writing—review and editing, M.P., N.B.-L. and A.P. All authors have read and agreed to the published version of the manuscript.

**Funding:** A.P. thanks the Spanish MINECO for project ref. PID2021-127423NB-I00.

**Data Availability Statement:** Not applicable.

**Acknowledgments:** The authors appreciate support of Iran Polymer and Petrochemical Institute (IPPI). A.P. is a Serra Húnter and thanks ICREA Academia 2019.

**Conflicts of Interest:** The authors declare no conflict of interest.

## References

1. Bahri-Laleh, N.; Hanifpour, A.; Mirmohammadi, S.A.; Poater, A.; Nekoomanesh-Haghighi, M.; Talarico, G.; Cavallo, L. Computational modeling of heterogeneous Ziegler-Natta catalysts for olefins polymerization. *Prog. Polym. Sci.* **2018**, *84*, 89–114. [[CrossRef](#)]
2. Rezaeian, A.; Hanifpour, A.; Teimoury, H.R.; Nekoomanesh-Haghighi, M.; Ahmadi, M.; Bahri-Laleh, N. Synthesis of Highly Spherical Ziegler-Natta Catalyst by Employing Span 80 as an Emulsifier Suitable for UHMWPE Production. *Polym. Bull.* **2022**. [[CrossRef](#)]
3. Piovano, A.; Groppo, E. Flexible ligands in heterogeneous catalysts for olefin polymerization: Insights from spectroscopy. *Coord. Chem. Rev.* **2022**, *451*, 214258. [[CrossRef](#)]
4. Mansouri, A.M.; Emami, M.; Yousefi, S.; Chen, C.; Gargari, M.H.; Hanifpour, A.; Bahri-Laleh, N. Structure–property relationship in film and blow molding type high-density polyethylene polymers from a slurry-process industrial plant. *J. Appl. Polym. Sci.* **2022**, *139*, e52877. [[CrossRef](#)]
5. Kuryndin, I.; Kostromin, S.; Mamalimov, R.; Chervov, A.; Grebennikov, A.; Bronnikov, S. Organic solvents effect on the physical and mechanical properties of polyethylene. *Polyolefins J.* **2022**, *9*, 25–31.
6. Yakimov, A.; Xu, J.; Searles, K.; Liao, W.-C.; Antinucci, G.; Friederichs, N.; Busico, V.; Copéret, C. DNP-SENS Formulation Protocols To Study Surface Sites in Ziegler–Natta Catalyst MgCl<sub>2</sub> Supports Modified with Internal Donors. *J. Phys. Chem. C* **2021**, *125*, 15994–16003. [[CrossRef](#)]
7. Piovano, A.; Signorile, M.; Braglia, L.; Torelli, P.; Martini, A.; Wada, T.; Takasao, G.; Taniike, T.; Groppo, E. Electronic Properties of Ti Sites in Ziegler–Natta Catalysts. *ACS Catal.* **2021**, *11*, 9949–9961. [[CrossRef](#)]
8. Tabrizi, M.; Sadjadi, S.; Pareras, G.; Nekoomanesh-Haghighi, M.; Bahri-Laleh, N.; Poater, A. Efficient hydro-finishing of polyalphaolefin based lubricants under mild reaction condition using Pd on ligands decorated halloysite. *J. Colloid Interface Sci.* **2021**, *581*, 939–953. [[CrossRef](#)]
9. Shams, A.; Sadjadi, S.; Duran, J.; Simon, S.; Poater, A.; Bahri-Laleh, N. Effect of support hydrophobicity of halloysite based catalysts on the PAO hydrofinishing performance. *Appl. Organomet. Chem.* **2022**, *36*, e6719. [[CrossRef](#)]
10. Hanifpour, A.; Bahri-Laleh, N.; Nekoomanesh-Haghighi, M.; Poater, A. Coordinative chain transfer polymerization of 1-decene in the presence of a Ti-based diamine bis (phenolate) catalyst: A sustainable approach to produce low viscosity PAOs. *Green Chem.* **2020**, *22*, 4617–4626. [[CrossRef](#)]
11. Hanifpour, A.; Bahri-Laleh, N.; Nekoomanesh-Haghighi, M.; Poater, A. Group IV diamine bis(phenolate) catalysts for 1-decene oligomerization. *Mol. Catal.* **2020**, *493*, 111047. [[CrossRef](#)]
12. Karimi, S.; Bahri-Laleh, N.; Sadjadi, S.; Pareras, G.; Nekoomanesh-Haghighi, M.; Poater, A. Pd on nitrogen rich polymer-halloysite nanocomposite as an environmentally benign and sustainable catalyst for hydrogenation of polyalphaolefin based lubricants. *J. Ind. Eng. Chem.* **2021**, *97*, 441–451. [[CrossRef](#)]
13. Fallah, M.; Bahri-Laleh, N.; Didehban, K.; Poater, A. Interaction of common cocatalysts in Ziegler-Natta catalyzed olefin polymerization. *Appl. Organomet. Chem.* **2020**, *34*, e5333. [[CrossRef](#)]
14. Shams, A.; Mehdizadeh, M.; Teimoury, H.-R.; Emami, M.; Mirmohammadi, S.A.; Sadjadi, S.; Bardaji, E.; Poater, A.; Bahri-Laleh, N. Effect of the Pore Architecture of Ziegler-Natta Catalyst on Its Behavior in Propylene/1-Hexene Copolymerization. *J. Ind. Eng. Chem.* **2022**. [[CrossRef](#)]
15. Ahmadi, M.; Nekoomanesh, M.; Arabi, H. A Simplified Comprehensive Kinetic Scheme for Modeling of Ethylene/1-butene Copolymerization Using Ziegler-Natta Catalysts. *Macromol. React. Eng.* **2010**, *4*, 135–144. [[CrossRef](#)]
16. McCoy, J.T.; Soares, J.B.P.; Rawatlal, R. Analysis of Slurry-Phase Co-Polymerization of Ethylene and 1-Butene by Ziegler–Natta Catalysts Part 1: Experimental Activity Profiles. *Macromol. React. Eng.* **2013**, *7*, 350–361. [[CrossRef](#)]
17. Mehdiabadi, S.; Lhost, O.; Vantomme, A.; Soares, J.B.P. Ethylene Polymerization Kinetics and Microstructure of Polyethylenes Made with Supported Metallocene Catalysts. *Ind. Eng. Chem. Res.* **2021**, *60*, 9739–9754. [[CrossRef](#)]
18. Hanifpour, A.; Hashemzadeh Gargari, M.; Rostami Daroukola, M.R.; Kalantari, Z.; Bahri-Laleh, N. Kinetic and microstructural studies of Cp<sub>2</sub>ZrCl<sub>2</sub> and Cp<sub>2</sub>HfCl<sub>2</sub>-catalyzed oligomerization of higher  $\alpha$ -olefins in mPAO oil base stocks production. *Polyolefins J.* **2021**, *8*, 31–40.
19. Domanskyi, S.; Gentekos, D.T.; Privman, V.; Fors, B.P. Predictive design of polymer molecular weight distributions in anionic polymerization. *Polym. Chem.* **2020**, *11*, 326–336. [[CrossRef](#)]
20. Walsh, D.J.; Schinski, D.A.; Schneider, R.A.; Guironnet, D. General route to design polymer molecular weight distributions through flow chemistry. *Nat. Commun.* **2020**, *11*, 3094. [[CrossRef](#)]
21. Ashuiev, A.; Humbert, M.; Norsic, S.; Blahut, J.; Gajan, D.; Searles, K.; Klose, D.; Lesage, A.; Pintacuda, G.; Raynaud, J.; et al. Spectroscopic Signature and Structure of the Active Sites in Ziegler–Natta Polymerization Catalysts Revealed by Electron Paramagnetic Resonance. *J. Am. Chem. Soc.* **2021**, *143*, 9791–9797. [[CrossRef](#)] [[PubMed](#)]

22. Saldívar-Guerra, E. Numerical Techniques for the Solution of the Molecular Weight Distribution in Polymerization Mechanisms, State of the Art. *Macromol. React. Eng.* **2020**, *14*, 2000010. [[CrossRef](#)]
23. Ali, A.; Jamil, M.I.; Uddin, A.; Hussain, M.; Aziz, T.; Tufail, M.K.; Guo, Y.; Jiang, B.; Fan, Z.; Guo, L. Kinetic and thermal study of ethylene-propylene copolymerization catalyzed by ansa-zirconocene activated with Alkylaluminium/borate: Effects of linear and branched alkylaluminium compounds as cocatalyst. *J. Polym. Res.* **2021**, *28*, 186.
24. Charoenpanich, T.; Anantawaraskul, S.; Soares, J.B.P.; Wongmahasirikun, P.; Shiohara, S. Modeling Propylene Polymerization in a Two-Reactor System: Model Development and Parameter Estimation. *Macromol. React. Eng.* **2022**. [[CrossRef](#)]
25. Kissin, Y.V.; Mink, R.I.; Nowlin, T.E.; Brandolini, A.J. Kinetics and mechanism of ethylene homopolymerization and copolymerization reactions with heterogeneous Ti-based Ziegler-Natta catalysts. *Top. Catal.* **1999**, *7*, 69–88. [[CrossRef](#)]
26. Soares, J.B.P. Mathematical modelling of the microstructure of polyolefins made by coordination polymerization: A review. *Chem. Eng. Sci.* **2001**, *56*, 4131–4153. [[CrossRef](#)]
27. Pladis, P.; Baltas, A.; Meimaroglou, D.; Kiparissides, C. A Dynamic Simulator for Slurry-Phase Catalytic Olefin Copolymerization in a Series of CSTRs: Prediction of Distributed Molecular and Rheological Properties. *Macromol. React. Eng.* **2018**, *12*, 1800017. [[CrossRef](#)]
28. Soares, J.B.P.; McKenna, T.F.L. A conceptual multilevel approach to polyolefin reaction engineering. *Can. J. Chem. Eng.* **2022**, *100*, 2432–2474. [[CrossRef](#)]
29. Burange, A.S.; Gawande, M.B.; Lam, F.L.Y.; Jayaram, R.V.; Luque, R. Heterogeneously catalyzed strategies for the deconstruction of high density polyethylene: Plastic waste valorisation to fuels. *Green Chem.* **2015**, *17*, 146–156. [[CrossRef](#)]
30. Urciuoli, G.; Vittoria, A.; Talarico, G.; Luise, D.; De Rosa, C.; Busico, V.; Cipullo, R.; Ruiz De Ballesteros, O.; Auriemma, F. In-Depth Analysis of the Nonuniform Chain Microstructure of Multiblock Copolymers from Chain-Shuttling Polymerization. *Macromolecules* **2021**, *54*, 10891–10902. [[CrossRef](#)]
31. Falivene, L.; Cavallo, L.; Talarico, G. Buried Volume Analysis for Propene Polymerization Catalysis Promoted by Group 4 Metals: A Tool for Molecular Mass Prediction. *ACS Catal.* **2015**, *5*, 6815–6822. [[CrossRef](#)]
32. Kulkarni, S.; Mishra, V.; Bontu, N.M. A comprehensive model for the micro and meso-scale level olefin polymerization: Framework and predictions. *Iran. Polym. J.* **2019**, *28*, 597–609. [[CrossRef](#)]
33. Khan, A.; Guo, Y.; Fu, Z.; Fan, Z. Kinetics of short-duration ethylene polymerization with MgCl<sub>2</sub>-supported Ziegler-Natta catalyst: Two-stage initiation evidenced by changes in active center concentration. *J. Appl. Polym. Sci.* **2017**, *137*, 45187. [[CrossRef](#)]
34. Jiang, B.; Weng, Y.; Zhang, S.; Zhang, Z.; Fu, Z.; Fa, Z. Kinetics and mechanism of ethylene polymerization with TiCl<sub>4</sub>/MgCl<sub>2</sub> model catalysts: Effects of titanium content. *J. Catal.* **2018**, *360*, 57–65. [[CrossRef](#)]
35. Wulkow, M. The simulation of molecular weight distributions in polyreaction kinetics by discrete Galerkin methods. *Macromol. Theory Simul.* **1996**, *5*, 393–416. [[CrossRef](#)]
36. Mehdiabadi, S.; Lhost, O.; Vantomme, A.; Soares, J.B.P. Ethylene/1-Hexene Copolymerization Kinetics and Microstructure of Copolymers Made with a Supported Metallocene Catalyst. *Macromol. React. Eng.* **2021**, *15*, 2100041. [[CrossRef](#)]
37. Soares, J.B.P.; Touloupidis, V. Polymerization kinetics and the effect of reactor residence time on polymer microstructure. In *Multimodal Polymers with Supported Catalysts*; Springer: Cham, Switzerland, 2019; pp. 115–153.
38. Reza, M.; Shamiri, A.; Azlan, M. Dynamic modeling and Molecular Weight Distribution of ethylene copolymerization in an industrial gas-phase Fluidized-Bed Reactor. *Adv. Powder Technol.* **2016**, *27*, 1526–1538.
39. Kang, J.; Shao, Z.; Chen, X.; Gu, X.; Feng, L. Fast and reliable computational strategy for developing a rigorous model-driven soft sensor of dynamic molecular weight distribution. *J. Process Control* **2017**, *56*, 79–99. [[CrossRef](#)]
40. Chen, X.; Shao, Z.; Gu, X.; Feng, L.; Biegler, L.T. Process Intensification of Polymerization Processes with Embedded Molecular Weight Distributions Models: An Advanced Optimization Approach. *Ind. Eng. Chem. Res.* **2018**, *58*, 6133–6145. [[CrossRef](#)]
41. Abedi, S.; Hosseinzadeh, M.; Kazemzadeh, M.A.; Daftari-Besheli, M. Effect of polymerization time on the molecular weight and molecular weight distribution of polypropylene. *J. Appl. Polym. Sci.* **2006**, *100*, 368–371. [[CrossRef](#)]
42. Floyd, S.; Choi, K.Y.; Taylor, T.W.; Ray, W.H. Polymerization of olefines through heterogeneous catalysis IV. Modeling of heat and mass transfer resistance in the polymer particle boundary layer. *J. Appl. Polym. Sci.* **1986**, *31*, 2231–2265. [[CrossRef](#)]
43. McKenna, T.F.; Soares, J.B.P. *Polyolefin Reaction Engineering*; Wiley-VCH: Weinheim, Germany, 2012.
44. Nassiri, H.; Arabi, H.; Hakim, S. Kinetic modeling of slurry propylene polymerization using a heterogeneous multi-site type ziegler-natta catalyst. *React. Kinet. Mech. Catal.* **2012**, *105*, 345–359. [[CrossRef](#)]
45. Najafi, M.; Parvazinia, M.; Ghoreishy, M.H.R.; Kiparissides, C. Development of a 2D Single Particle Model to Analyze the Effect of Initial Particle Shape and Breakage in Olefin Polymerization. *Macromol. React. Eng.* **2014**, *8*, 29–45. [[CrossRef](#)]
46. Thompson, D.E. Modelling of Molecular Weight Distributions in Ziegler-Natta Catalyzed Ethylene Copolymerizations. Ph.D. Thesis, Queen's University, Kingston, ON, Canada, 2009.
47. Tongtummachat, T.; Ma-In, R.; Anantawaraskul, S.; Soares, J.B.P. Dynamic Monte Carlo Simulation for Chain-Shuttling Polymerization of Olefin Block Copolymers in Continuous Stirred-Tank Reactor. *Macromol. React. Eng.* **2020**, *14*, 2000030. [[CrossRef](#)]
48. Kissin, Y.V. *Alkene-Polymerization-Reactions-with-Transition-Metal-Catalysts*; Elsevier Science & Technology: Oxford, UK, 2008; Volume 173.
49. Kissin, Y.V. Main kinetic features of ethylene polymerization reactions with heterogeneous Ziegler-Natta catalysts in the light of a multicenter reaction mechanism. *J. Polym. Sci. Part A Polym. Chem.* **2001**, *39*, 1681–1695. [[CrossRef](#)]

50. Kissin, Y.V. Molecular Weight Distributions of linear Polymers: Detailed Analysis from GPC Data. *J. Polym. Sci. Part A Polym. Chem.* **1995**, *33*, 227–237. [[CrossRef](#)]
51. Kissin, Y.V.; Brandolini, A.J. Ethylene Polymerization Reactions with Ziegler–Natta Catalysts. II. Ethylene Polymerization Reactions in the Presence of Deuterium. *J. Polym. Sci. Part A Polym. Chem.* **2000**, *37*, 4273–4280. [[CrossRef](#)]
52. Choi, Y.; Soares, J.B.P. Supported single-site catalysts for slurry and gas-phase olefin polymerisation. *Can. J. Chem. Eng.* **2012**, *90*, 646–671. [[CrossRef](#)]
53. Khan, M.J.H.; Hussain, M.A.; Mujtaba, I.M. Multiphase reaction modeling for polypropylene production in a pilot-scale catalytic reactor. *Polymers* **2016**, *8*, 220. [[CrossRef](#)]
54. Wells, G.J.; Harmon Ray, W. Prediction of polymer properties in LDPE reactors. *Macromol. Mater. Eng.* **2005**, *290*, 319–346. [[CrossRef](#)]
55. McKenna, T.F.; Soares, J.B.P. Single particle modelling for olefin polymerization on supported catalysts: A review and proposals for future developments. *Chem. Eng. Sci.* **2001**, *56*, 3931–3949. [[CrossRef](#)]
56. Floyd, S.; Choi, K.Y.; Taylor, T.W.; Ray, W.H. Polymerization of olefins through heterogeneous catalysis. III. Polymer particle modelling with an analysis of intraparticle heat and mass transfer effects. *J. Appl. Polym. Sci.* **1986**, *32*, 2935–2960. [[CrossRef](#)]
57. Floyd, S.; Heiskanen, T.; Taylor, T.W.; Mann, G.E.; Ray, W.H. Polymerization of olefins through heterogeneous catalysis. VI. Effect of particle heat and mass transfer on polymerization behavior and polymer properties. *J. Appl. Polym. Sci.* **1987**, *33*, 1021–1065. [[CrossRef](#)]
58. Kissin, Y.V. Active centers in Ziegler–Natta catalysts: Formation kinetics and structure. *J. Catal.* **2012**, *292*, 188–200. [[CrossRef](#)]
59. Najafi, M.; Parvazinia, M.; Ghoreishy, M.H.R. Modelling the catalyst fragmentation pattern in relation to molecular properties and particle overheating in olefin polymerization. *Polyolefins J.* **2014**, *1*, 77–91.
60. Das, T.K.; Poater, A. Review on Use of Heavy Metal Deposits from Water Treatment Waste towards Catalytic Chemical Syntheses. *Int. J. Mol. Sci.* **2021**, *22*, 13383. [[CrossRef](#)]
61. Altass, H.M.; Khder, A.S.; Ahmed, S.A.; Morad, M.; Alsabei, A.A.; Jassas, R.S.; Althagafy, K.; Ahmed, A.I.; Salama, R.S. Highly efficient, recyclable cerium-phosphate solid acid catalysts for the synthesis of tetrahydrocarbazole derivatives by Borsche–Drechsel cyclization. *Reac. Kinet. Mech. Cat.* **2021**, *134*, 143–161. [[CrossRef](#)]
62. Salama, R.S.; El-Bahy, S.M.; Mannaa, M.A. Sulfamic acid supported on mesoporous MCM-41 as a novel, efficient and reusable heterogenous solid acid catalyst for synthesis of xanthene, dihydropyrimidinone and coumarin derivatives. *Colloids Surf. A Physicochem. Eng.* **2021**, *628*, 127261. [[CrossRef](#)]
63. Altass, H.M.; Morad, M.; Khder, A.S.; Raafat, M.; Alsantali, R.I.; Khder, M.A.; Salama, R.S.; Shaheer Malik, M.; Moussa, Z.; Abourehab, M.A.S.; et al. Exploitation the unique acidity of novel cerium-tungstate catalysts in the preparation of indole derivatives under eco-friendly acid catalyzed Fischer indole reaction protocol. *Arab. J. Chem.* **2022**, *15*, 103670. [[CrossRef](#)]
64. Luo, Z.-H.; Zheng, Y.; Cao, Z.-K.; Wen, S.H. Mathematical Modeling of the Molecular Weight Distribution of Polypropylene Produced in a Loop Reactor. *Polym. Eng. Sci.* **2007**, *47*, 1643–1649. [[CrossRef](#)]